PCCP

ROYAL SOCIETY OF CHEMISTRY

COMMUNICATION

View Article Online
View Journal | View Issue

Cite this: *Phys. Chem. Chem. Phys.*, 2022, **24**, 22431

Received 4th July 2022,
Accepted 4th September 2022

DOI: 10.1039/d2cp03030f

rsc.li/pccp

Effect of temperature gradient on quantum transport

Amartya Bose *[a] and Peter L. Walters [bc]

The recently introduced multisite tensor network path integral (MS-TNPI) method [Bose and Walters, *J. Chem. Phys.*, 2022, 156, 24101] for simulating quantum dynamics of extended systems has been shown to be effective in studying one-dimensional systems coupled with local baths. Quantum transport in these systems is typically studied at a constant temperature. However, temperature seems to be a very obvious parameter that can be spatially changed to control this transport. Here, MS-TNPI is used to study the "non-equilibrium" effects of an externally imposed temperature profile on the excitonic transport in one-dimensional Frenkel chains coupled with local vibrations. We show that in addition to being important for incorporating heating effects of excitation by lasers, temperature can also be an interesting parameter for quantum control.

Quantum transport in extended open systems has been one of the holy-grails of quantum dynamics. It combines the difficulty of treating extended quantum systems with the difficulty of treating open quantum systems, both of which potentially lead to exponential growth of computational complexity. However, such systems are ubiquitous in nature, and hence, are of great importance. From magnetic materials to molecular aggregates, a vast variety of interesting physical phenomena lend themselves to be modeled as extended one-dimensional quantum systems interacting with open thermal environments. Wave function-based methods such as density matrix renormalization group[1–6] (DMRG) and multi-configuration time-dependent Hartree[7–9] (MCTDH and ML-MCTDH) and related methods have proven to be exceptionally useful in simulating the quantum dynamics of extended systems. However, due to their computational complexity, these methods are typically less useful when it comes to simulations of open systems.

Path integral methods have often been presented as a viable solution to the problem of calculating and storing the wave functions for open systems. With these methods, the main challenge is that the number of paths considered in the path integral increases exponentially with the number of time steps. However, this exponential proliferation of the system path list can be curtailed through the use of an iterative procedure that exploits the rapid decay of correlation between well-separated time points. Although the computational complexity still increases exponentially with the number of time points retained within memory (L), this is usually much smaller then the typical number of time points in the simulation. Thus, the quasi-adiabatic propagator path integral[10–13] (QuAPI) methods, which are based on Feynman–Vernon influence functional,[14] make simulations of general open quantum systems much more approachable. Of late, the usage of tensor networks to facilitate simulations with influence functionals has also become quite common.[15–18] Ideas from these tensor network-based influence functional methods have motivated a recent extension of DMRG to simulating the non-equilibrium dynamics of extended open quantum systems.[19] This multisite tensor network path integral (MS-TNPI) method has also been used to explore the dynamics and spectrum of the B850 ring of the light harvesting subsystem[20] and study the effects of phononic scattering on spin transport.[21]

Despite their utility, the application of traditional path integral methods to extended open quantum systems suffers hugely from exponential scaling stemming from two different sources. First, the dimensionality of the system scales exponentially with the number of "units" or "entities" involved. Suppose we have a setup involving P units each with dimensionality d, then the total dimensionality of the system is d^P. Additionally, the presence of thermal environments renders the dynamics non-Markovian. Consequently, there is an exponential scaling with respect to the number of time steps within memory. The base of this exponential scaling is related to the dimensionality

[a] *Department of Chemistry, Princeton University, Princeton, New Jersey 08544, USA. E-mail: amartyab@princeton.edu, amartya.bose@gmail.com*
[b] *Department of Chemistry, University of California, Berkeley, California 94720, USA*
[c] *Miller Institute for Basic Research in Science, University of California Berkeley, Berkeley, California 94720, USA. E-mail: peter.l.walters2@gmail.com*

of the system. So, if the memory length is L for this hypothetical problem, the computational complexity would go as $\mathcal{O}\left((d^P)^{2L}\right)$. This is the issue that MS-TNPI addresses by using a DMRG-like decomposition of the system along the various sites in addition to a decomposition of the "paths" along the temporal dimension.

The present paper uses MS-TNPI to explore the effects of temperature differences on excitonic transport in extended open systems. Such temperature differences can be caused by an external temperature gradient being applied across a molecular wire or more commonly as a side-effect of heat generated during laser-induced excitations. Thus, to accurately simulate such phenomena, one would need to worry about spatially inhomogeneous temperatures. In addition, we want to explore the possibilities of using non-constant temperature profiles as a potentially useful parameter for controlling and changing the characteristics of the quantum transport.

Method

In this work, we use the well-known Frenkel form with nearest neighbor couplings to explore the effects of non-constant temperature profiles on exciton transport. The Hamiltonian for a system with P units is given by

$$\hat{H}_0 = \varepsilon \sum_{j=1}^{P} |e_j\rangle\langle e_j| + \hbar J \sum_{j=1}^{P-1} \left(|e_j\rangle\langle e_{j+1}| + |e_j\rangle\langle e_{j+1}|\right), \qquad (1)$$

where $\hbar J$ is the excitonic coupling between the neighboring sites, ε is the excitation energy of the sites and lastly, $|e_j\rangle$ is the many-body wavefunction with just the jth site excited. In terms of the one-body ground, $|\phi_j^g\rangle$, and excited, $|\phi_j^e\rangle$, wavefunctions, $|e_j\rangle = \left|\phi_j^e\right\rangle \otimes \prod_{k\neq j} |\phi_k^g\rangle$.

Typically, for simulations of extended systems, DMRG and DMRG-like methods proceed by decomposing the system along the spatial dimension. By exploiting the lack of correlation between distant sites, the resulting matrix product state (MPS) can be an extremely compact and efficient representation of the system. The reduced density matrix after the nth time step can expressed in the form of an MPS as follows

$$\tilde{\rho}\left(S_n^{\pm}, n\Delta t\right) = \sum_{\{\alpha_{(j,n)}\}} A^{s_{1,n}^{\pm}}_{\alpha_{(1,n)}} A^{s_{2,n}^{\pm}}_{\alpha_{(1,n)},\alpha_{(2,n)}} \cdots A^{s_{P,n}^{\pm}}_{\alpha_{(P-1,n)}}, \qquad (2)$$

where $\alpha_{j,n}$ is the index connecting the jth site at time-step n to the $(j+1)$ th site at the same time step. Fig. 1 gives a graphical representation of this structure. In this work, the forward–backward state of the jth site at the nth time point is denoted by $s_{j,n}^{\pm}$ and the states of all the sites at this time step are collectively represented by $S_n^{\pm}$. (Here, the forward–backward state is a combination of the forward, bra, and backward, ket, states of the density matrix.) When the density matrix is represented as an MPS, the forward-backward propagator, which evolves it in time, must be represented as a matrix product operator (MPO). The forward–backward propagator MPO corresponding to the Hamiltonian in eqn (1) can be obtained using a second-order time-evolved block decimation scheme.[19]

Fig. 1 Schematic of a density matrix of an extended system represented as an MPS.

With this setup, it is possible to obtain the time-dynamics of the isolated system through a series of MPO-MPS applications. However, often the individual sites interact with separate dissipative environments. These environments can, under Gaussian response theory, be mapped onto baths of N_{osc} harmonic oscillators each, yielding the full system-environment Hamiltonian as:

$$\hat{H} = \hat{H}_0 + \sum_{j=1}^{P} \sum_{l=1}^{N_{\text{osc}}} \frac{p_{jl}^2}{2m_{jl}} + \frac{1}{2} m_{jl}\omega_{jl}^2 \left(x_{jl} - \frac{c_{jl}\hat{s}_j}{m_{jl}\omega_{jl}^2}\right)^2, \qquad (3)$$

where $\hat{H}_0$ is the Hamiltonian corresponding to the isolated extended system with P units or particles, eqn (1). The lth harmonic oscillator of the jth system unit interacts with it through the operator $\hat{s}_j$ with a strength of c_{jl}. For excitonic applications, $\hat{s}_j$ is defined as $\hat{s}_j|\phi_j^e\rangle = |\phi_j^e\rangle$ and $\hat{s}_j|\phi_j^g\rangle = 0$. The combination of a Frenkel system with vibrations as in eqn (3) is often referred to as the Frenkel–Holstein model in the literature. The frequencies and couplings of the baths are given in terms of the spectral density,

$$\mathcal{J}_j(\omega) = \frac{\pi}{2} \sum_{l=1}^{N_{\text{osc}}} \frac{c_{lj}^2}{m_{lj}\omega_{lj}} \delta\left(\omega - \omega_{lj}\right). \qquad (4)$$

This can be related to the energy gap autocorrelation function,[22,23] which can be approximated through classical trajectory-based methods.[24,25] These dissipative baths, most commonly, encode the effects of the phonons on the excitonic dynamics.

In the presence of the dissipative environment, the time evolution of the reduced density matrix can be described as

$$\tilde{\rho}\left(S_N^{\pm}, N\Delta t\right) = \sum_{S_0^{\pm}} \sum_{S_1^{\pm}} \cdots \sum_{S_{N-1}^{\pm}} \tilde{\rho}\left(S_0^{\pm}, 0\right) P_{S_0^{\pm}\cdots S_N^{\pm}} \qquad (5)$$

$$= \sum_{S_0^{\pm}} \sum_{S_1^{\pm}} \cdots \sum_{S_{N-1}^{\pm}} \tilde{\rho}(S_0^{\pm}, 0) P^{(0)}_{S_0^{\pm}\cdots S_N^{\pm}} F\left[\left\{S_n^{\pm}\right\}\right]. \qquad (6)$$

Here, $P^{(0)}_{S_0^{\pm}\cdots S_N^{\pm}}$ is the bare path amplitude tensor, which contains the full information of the isolated system, and F is the Feynman–Vernon influence functional,[14] which depends on the temperature and the spectral density, and encodes the system-environment interaction. Lastly, $P_{S_0^{\pm}\cdots S_N^{\pm}}$ is the path amplitude tensor, which describes the system in the presence of the solvent. For the problems with temperature gradients explored here, the bare path amplitude tensor, being independent of temperature, does not cause the difference in dynamics. The Feynman–Vernon influence functional is the only thing that changes with the sites because of the gradient. The system dynamics gets affected as a

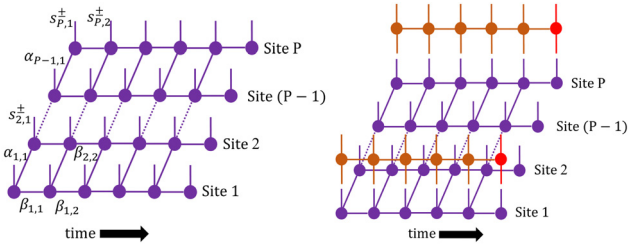

(a) 2D MS-TNPI tensor network. **(b)** Incorporation of influence functional.

Fig. 2 Schematic of MS-TNPI tensor network. (Schematics reproduced from ref. 20.)

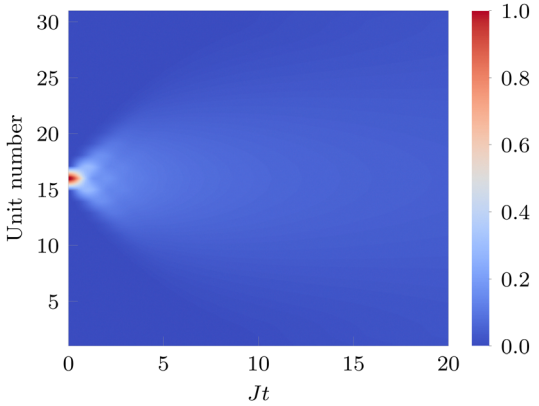

Fig. 3 Unit dependent excited state population, $\bar{P}_j^{\mathrm{exc}}(t)$, when no temperature gradient is applied.

consequence. Since the dimensionality of the path amplitude tensor grows exponentially with the number of particles and time steps, it can only be explicitly constructed in a very small number of cases.

MS-TNPI[19] avoids this exponential scaling by performing a spatial decomposition of the bare system and combining it with a temporal decomposition of the influence functional to produce a compact two-dimensional tensor network representation of the path amplitude tensor,

$$P_{S_0^{\pm}\cdots S_N^{\pm}} = \sum_{\{\beta_n\}} \mathbb{T}_{\beta_0}^{S_0^{\pm}} \cdots \mathbb{T}_{\beta_{n-1},\beta_n}^{S_n^{\pm}} \cdots \mathbb{T}_{\beta_{N-1}}^{S_N^{\pm}}. \tag{7}$$

Here, β_n is the index connecting the tensors at time-point n to the ones at $n+1$, and each $\mathbb{T}$ is a matrix product representation decomposed along the site axis. The resulting two-dimensional tensor network is shown in Fig. 2(a). Each of the columns roughly contains the state of the full system at any point of time. Therefore, when contracting the network along the columns, we get the full reduced density matrix corresponding to the extended system. Naïvely speaking, the number of columns in the MS-TNPI network corresponds to the total length of the simulation. However, an iterative procedure can be employed that effectively reduces the number columns to the length of the memory induced by the baths. The rows represent the path amplitude corresponding to the individual sites or units of the system. This allows both the incorporation of the Feynman–Vernon influence functional in a transparent manner as MPOs acting on the rows as shown in Fig. 2(b) and the truncation of memory.

Numerical examples

As our first example, we consider a $P = 31$ site system with $\hbar J = 1$ and $\varepsilon = 100$. (The sites are numbered from 1 to 31.) We are interested in the effects of thermal inhomogeneities and not the differences in the structure of the vibronic couplings. Therefore, in this work, the spectral densities, which characterize the interaction between the vibrational bath and the electronic system, are taken to be site independent. For the current example, the spectral density is

$$\mathcal{J}_j(\omega) = 2\pi\hbar\xi\omega \exp\left(-\frac{\omega}{\omega_c}\right), \tag{8}$$

where $\omega_c = 8J$ is the cutoff frequency and the dimensional Kondo parameter, $\xi = 0.075$. We start the discussion by considering the dynamics of the exciton under a constant temperature of $k_B T = \hbar J$. Consider an initial state where the middle monomer is excited, $\tilde{\rho}(0) = |e_{16}\rangle\langle e_{16}|$. The excited state population dynamics, $\bar{P}_j^{\mathrm{exc}}(t) = \langle \phi_j^e | \tilde{\rho}(t) | \phi_j^e \rangle$, is demonstrated in Fig. 3. Because the middle unit is initially excited, the dynamics is completely symmetric, that is the populations of the units equidistant from the edges are identical. (A short explanation of the notation used: we use $\bar{P}^{\mathrm{exc}}$ when denoting the dynamics in absence of a temperature gradient. When a temperature gradient is applied, we refer to it as P^{exc}.)

Now, consider applying a temperature gradient of $0.05\hbar J/k_B$ with an average temperature of $k_B\bar{T} = \hbar J$. The temperature is lowest at the bottom end where the units have lower numbers, and rises as we move up. The application of this temperature gradient breaks the symmetry discussed in the previous paragraph. To explore this deviation numerically, we introduce the following measure:

$$\delta P_j^{\mathrm{exc}}(t) = \frac{P_j^{\mathrm{exc}}(t) - \bar{P}_j^{\mathrm{exc}}(t)}{\bar{P}_j^{\mathrm{exc}}(t)} \times 100. \tag{9}$$

Here, $\bar{P}^{\mathrm{exc}}$ is the same dynamics as discussed in the previous paragraph and shown in Fig. 3. The deviation from the zero-gradient dynamics is shown for this particular case in Fig. 4. For the linear ramp considered, the transport process seems to preferentially move the exciton to the colder monomers. The deviations are quite significant with an upper limit of around ±75%. (These calculations took roughly 2.5 hours on an Intel Xeon Gold CPU with 32 cores.)

As a more realistic example of exciton transfer, consider a chain of 31 bacteriochlorophyll (BChl) units. The intermonomer electronic coupling, $\hbar J$, is taken to be 156.5 cm^{-1} and the excitation energy of a BChl unit, ε, is taken to be 12 390 cm^{-1}. The local spectral density was calculated from the molecular dynamics-based (MD) bath response function, $C_{\mathrm{MD}}(t)$, reported in ref. 26 using the following relation:

$$\mathcal{J}_j(\omega) = \frac{\hbar\omega\beta_{\mathrm{MD}}}{2}\int_0^{\infty} C_{\mathrm{MD}}(t)\cos(\omega t)\mathrm{d}t. \tag{10}$$

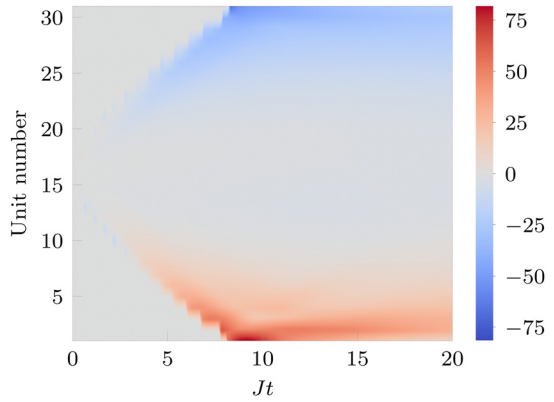

Fig. 4 Plot of $\delta P_j^{\mathrm{exc}}(t)$ in presence of a temperature gradient of $0.05\hbar J/k_B$ per site.

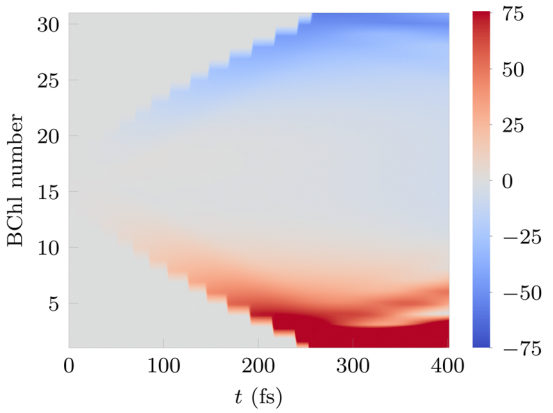

Fig. 6 Plot of $\delta P_j^{\mathrm{exc}}(t)$ for a chain of BChl molecules caused by an external temperature gradient of 10 K per unit.

The resultant spectral density is shown in Fig. 5. (Note that the inverse temperature used here, β_{MD}, corresponds to MD simulation setup. In addition, the relation between the spectral density and the MD correlation function used here, eqn (10), and the one reported in ref. 26 are different. It has been shown that eqn (10) is better at preserving the temperature invariance of the spectral density.[27])

The spectral density, eqn (10), is independent of the temperature of the path integral simulations done here. So, just as in the previous example, all the monomer units have identical spectral densities here as well. We want to understand the changes brought about in the dynamics through an external temperature gradient of 10 K per unit. The average temperature of the chain is held at 300 K. Fig. 6 shows the difference caused in the excitonic population dynamics by the externally imposed temperature gradient. Note that despite having a structured spectral density, the trends here are identical to the model example, Fig. 4. Even in this case, population preferentially moves towards the colder end of the chain.

Till now, we have considered the impact of a linear external temperature gradient on the dynamics. To use temperature differences as a parameter for quantum control, one would like to impose non-trivial temperature profiles as well. For the model Ohmic bath, eqn (8), consider two such non-linear temperature profiles:

(1) The temperature rises as a Gaussian at the point where the initial excitation is located (16th site for instance). This will be called the heating profile.

(2) The temperature decreases as an inverted Gaussian at the point where the initial excitation is located. This will be called the cooling profile.

These are shown in Fig. 7. Temperature profile (1), the heating profile, is closely related to what would happen if a laser was used to cause the initial excitation. In this case, along with the electronic excitation, heat would also be dumped into the vibrational degrees of freedom of the middle and nearby monomers. The deviations in excitonic population corresponding to these two temperature profiles is shown in Fig. 8.

The drop in temperature associated with the cooling profile seems to force a faster excitonic transfer away from the cold middle site. The reverse happens when the initially excited site is at a higher temperature. The heating profile allows the middle monomers to hold on to the exciton longer than when no temperature profile is imposed. It is interesting to note that this behavior seems to go against the movement of excitons to colder regions in presence of linear temperature ramps that we

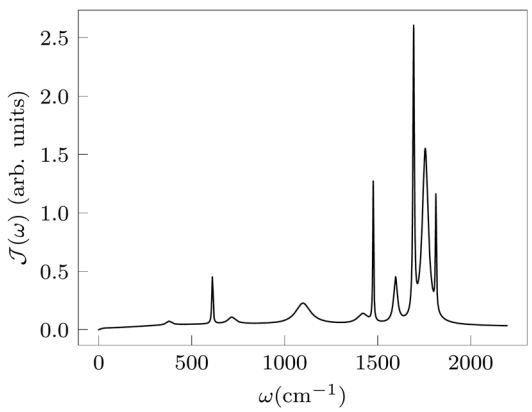

Fig. 5 Spectral density describing the thermal environment of the bacteriochlorophyll molecules. It was obtained by using eqn (10) on the bath response function reported in ref. 26.

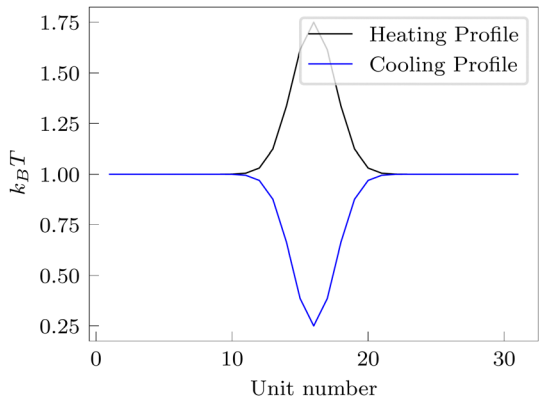

Fig. 7 Different temperature profiles.

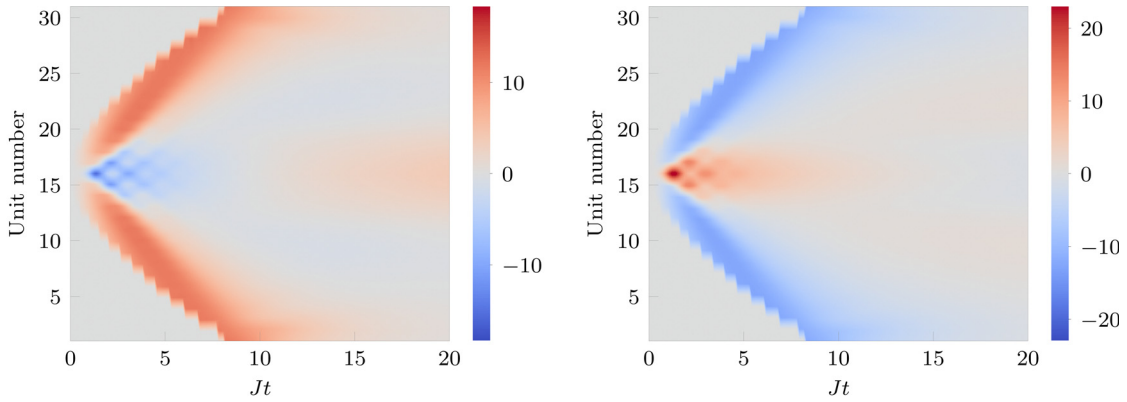

(a) Temperature profile (1): Heating profile.

(b) Temperature profile (2): Cooling profile.

Fig. 8 Plots of $\delta P_j^{exc}(t)$ corresponding to different temperature profiles.

previously demonstrated. One may hypothesize that the second derivative of the temperature profile with the units is what affects the change. Further research investigating this phenomenon will be conducted in the future.

Concluding remarks

We have demonstrated a noticeable change in the quantum transport of excitons in the presence of an externally imposed temperature profile. When the temperature increases linearly with the units, the excitonic population seems to travel preferentially to the colder end of the chain. This trend is consistent between model spectral densities and structured ones derived from molecular dynamics simulations. Thus, the hope is that one may be able to control aspects of the transport using the temperature profile. We have demonstrated that when we locally heat or cool the Frenkel chain, the rate of transfer of the exciton changes. Future work would look into the impact of the shape of the temperature profile. Is it enough to heat or cool particular parts of the chain or does the exact function mapping the units to their corresponding temperature also matter? Investigations on the effect of temperature differences on spectra and other properties will also be undertaken in the future. We noted how the behavior of the exciton changes from a constant gradient temperature profile to a non-constant gradient temperature profile. This has potential for being exploited in vibrationally trapping excitons in certain regions of space. This feature would also be an important aspect of our explorations in the future. In addition, it has recently been shown that the presence of phononic scattering in the closely-related XXZ spin chain makes transport diffusive.[21] We are also going to explore of the effect of temperature gradients on diffusion constants for the quantum transport. Ultimately, what has been shown in this communication seems to indicate that temperature might be a useable control for quantum dynamics. Further exploration to this end would be done in the future.

Author contributions

Both authors contributed equally to the design, implementation and writing of this communication.

Conflicts of interest

There are no conflicts to declare.

Acknowledgements

A. B. acknowledges the support of the Computational Chemical Science Center: Chemistry in Solution and at Interfaces funded by the US Department of Energy under Award No. DE-SC0019394. P. W. acknowledges the Miller Institute for Basic Research in Science for funding.

Notes and references

1 S. R. White, *Phys. Rev. Lett.*, 1992, **69**, 2863–2866.
2 S. R. White and A. E. Feiguin, *Phys. Rev. Lett.*, 2004, **93**, 076401.
3 U. Schollwöck, *Rev. Mod. Phys.*, 2005, **77**, 259–315.
4 U. Schollwöck, *Philos. Trans. R. Soc., A*, 2011, **369**, 2643–2661.
5 J. Ren, Z. Shuai and G. Kin-Lic Chan, *J. Chem. Theory Comput.*, 2018, **14**, 5027–5039.
6 S. Paeckel, T. Köhler, A. Swoboda, S. R. Manmana, U. Schollwöck and C. Hubig, *Ann. Phys.*, 2019, **411**, 167998.
7 M. Beck, *Phys. Rep.*, 2000, **324**, 1–105.
8 H. Wang and M. Thoss, *J. Chem. Phys.*, 2003, **119**, 1289–1299.
9 F. D. Maiolo, G. A. Worth and I. Burghardt, *J. Chem. Phys.*, 2021, **154**, 144106.
10 N. Makri and D. E. Makarov, *J. Chem. Phys.*, 1995, **102**, 4600–4610.
11 N. Makri and D. E. Makarov, *J. Chem. Phys.*, 1995, **102**, 4611–4618.
12 N. Makri, *J. Chem. Phys.*, 2018, **149**, 214108.
13 N. Makri, *J. Chem. Theory Comput.*, 2020, **16**, 4038–4049.
14 R. P. Feynman and F. L. Vernon, *Ann. Phys.*, 1963, **24**, 118–173.
15 A. Strathearn, P. Kirton, D. Kilda, J. Keeling and B. W. Lovett, *Nat. Commun.*, 2018, **9**, 1–9.

16 M. R. Jørgensen and F. A. Pollock, *Phys. Rev. Lett.*, 2019, **123**, 240602.
17 A. Bose and P. L. Walters, 2021, *arXiv*, 2021, preprint, *arXiv*:2106.12523.
18 A. Bose, *Phys. Rev. B*, 2022, **105**, 024309.
19 A. Bose and P. L. Walters, *J. Chem. Phys.*, 2022, **156**, 24101.
20 A. Bose and P. L. Walters, *J. Chem. Theory Comput.*, 2022, **18**, 4095–4108.
21 A. Bose, *Effect of Phonons and Impurities on the Quantum Transport in XXZ Spin-Chains*, 2022, **https://arxiv.org/abs/2206.11156**.
22 N. Makri, *J. Phys. Chem. B*, 1999, **103**, 2823–2829.
23 A. Bose, *J. Chem. Phys.*, 2022, **157**, 054107.
24 J. Cao and G. A. Voth, *J. Chem. Phys.*, 1994, **100** 5106–5117.
25 I. R. Craig and D. E. Manolopoulos, *J. Chem. Phys.*, 2004, **121**, 3368–3373.
26 C. Olbrich and U. Kleinekathöfer, *J. Phys. Chem. B*, 2010, **114**, 12427–12437.
27 S. Valleau, A. Eisfeld and A. Aspuru-Guzik, *J. Chem. Phys.*, 2012, **137**, 224103.

